# Craniosynostosis in transgenic mice overexpressing *Nell-1*

Xinli Zhang,[1] Shun'ichi Kuroda,[2] Dale Carpenter,[3] Ichiro Nishimura,[4] Chia Soo,[5] Rex Moats,[6] Keisuke Iida,[4] Eric Wisner,[7] Fei-Ya Hu,[8] Steve Miao,[1] Steve Beanes,[5] Catherine Dang,[5] Heleni Vastardis,[9] Michael Longaker,[10] Katsuyuki Tanizawa,[2] Norihiro Kanayama,[2] Naoaki Saito,[11] and Kang Ting[1,5]

[1]Dental and Craniofacial Research Institute, University of California, Los Angeles, Los Angeles, California, USA
[2]Institute of Scientific and Industrial Research, Osaka University, Ibaraki, Japan
[3]Department of Neurology, University of California, Irvine, Irvine, California, USA
[4]The Jane and Jerry Weintraub Center for Reconstructive Biotechnology, and
[5]Department of Surgery, University of California, Los Angeles, Los Angeles, California, USA
[6]Department of Radiology, Children's Hospital, Los Angeles, California, USA
[7]Department of Surgical and Radiological Sciences, School of Veterinary Medicine, University of California, Davis, Davis, California, USA
[8]Chang-Gung Memorial Hospital, Taipei, Taiwan
[9]School of Dentistry, Tufts University, Boston, Massachusetts, USA
[10]Department of Surgery, Stanford University, Stanford, California, USA
[11]Biosignal Research Center, Kobe University, Kobe, Japan

**Previously, we reported *NELL-1* as a novel molecule overexpressed during premature cranial suture closure in patients with craniosynostosis (CS), one of the most common congenital craniofacial deformities. Here we describe the creation and analysis of transgenic mice overexpressing *Nell-1*. *Nell-1* transgenic animals exhibited CS-like phenotypes that ranged from simple to compound synostoses. Histologically, the osteogenic fronts of abnormally closing/closed sutures in these animals revealed calvarial overgrowth and overlap along with increased osteoblast differentiation and reduced cell proliferation. Furthermore, anomalies were restricted to calvarial bone, despite generalized, non-tissue-specific overexpression of *Nell-1*. In vitro, *Nell-1* overexpression accelerated calvarial osteoblast differentiation and mineralization under normal culture conditions. Moreover, *Nell-1* overexpression in osteoblasts was sufficient to promote alkaline phosphatase expression and micronodule formation. Conversely, downregulation of Nell-1 inhibited osteoblast differentiation in vitro. In summary, *Nell-1* overexpression induced calvarial overgrowth resulting in premature suture closure in a rodent model. *Nell-1*, therefore, has a novel role in CS development, perhaps as part of a complex chain of events resulting in premature suture closure. On a cellular level, *Nell-1* expression may modulate and be both sufficient and required for osteoblast differentiation.**

*J. Clin. Invest.* **110**:861–870 (2002). doi:10.1172/JCI200215375.

## Introduction

Craniosynostosis (CS), the premature closure of cranial sutures, affects 1 in 3,000 infants and therefore is one of the most common human congenital craniofacial deformities (1). Premature suture closure, which results in cranial dysmorphism, can be either familial or sporadic in origin (1). Neither gender nor ethnicity can be used to predict which infants will be affected. Although genetic linkage analyses of CS-related syndromes have provided a wealth of new information about the molecular control of suture formation, the biology of local suture closure, especially in nonsyndromic, nonfamilial CS, is still largely unknown.

Presently, more than 85 human mutations, which produce various familial CS syndromes, have been localized to the FGF receptor genes *FGFR1, FGFR2,* and *FGFR3*. All are "gain-of-function" mutations that result in increased receptor activity (1). No human CS syndromes have been linked to the FGF ligands; however, several animal models of CS have been associated with FGF overexpression (2, 3). The only described *MSX2* mutation associated with CS (4) also results in increased *MSX2* activity (5–7). While these candidate genes are known to play important roles in osteoblast proliferation and differentiation, they also have more generalized roles during embryogenesis. Thus, it is not surprising that transgenic mouse models with mutations in these genes often manifest extracranial abnormalities not observed in the majority of patients with CS (1, 2, 8).

*Received for publication March 1, 2002, and accepted in revised form July 16, 2002.*

**Address correspondence to:** Kang Ting, Center for the Health Sciences 30-113, University of California, Los Angeles, 10833 Le Conte Avenue, Los Angeles, California 90095, USA. Phone: (310) 206-6305; Fax: (310) 206-5349; E-mail: kting@ucla.edu.

**Conflict of interest:** No conflict of interest has been declared.

**Nonstandard abbreviations used:** craniosynostosis (CS); FGF receptor (FGFR); cytomegalovirus, (CMV); magnetic resonance imaging (MRI); adenovirus (Ad); embryonic day 18 (E18); β-Galactosidase (β-Gal); fetal rat calvarial cell (FRCC); transgenic $F_2$ ($TF_2$); normal $F_2$ ($NF_2$); posterior-frontal (PF); microcomputerized tomography (MCT).

Premature suture closure in human CS can be divided into two possibly distinct processes: calvarial overgrowth and bony fusion. While calvarial overgrowth may be essential to bringing the two opposing osteogenic fronts into proximity in order to induce bony fusion, it does not necessarily follow that calvarial overgrowth or overlap alone will result in bony fusion. Thus, the study of premature suture closure mechanisms must include study of both abnormal suture overgrowth/overlap and bony fusion (6).

Recently, FGF2 and FGFR1 have been implicated in premature cranial suture fusion via *CBFA1*-mediated pathways (8). Missense mutation of CBFA1 is linked to cleidocranial dysplasia, manifested as delayed suture closure (9). Therefore, examination of *Cbfa1* (*Runx2*), a downstream target of *Fgfr1* that is essential for bone formation, may be key to understanding the signaling cascade in CS. In addition, *Msx2*, a member of the highly conserved *Msx* homeobox gene family with pleiotropic effects in development, has been implicated in an animal model of CS (5, 6). Specifically, increased osteogenic cell proliferation has been proposed as a mechanism for premature suture closure in *Msx2*-overexpressing transgenic mice, which exhibit suture overgrowth/overlap without suture fusion.

To elucidate the molecular pathway for suture closure, we previously used differential display to identify genes that were specifically upregulated within abnormally fused sutures in patients with nonfamilial, nonsyndromic CS. We isolated and characterized NELL-1, which is a Nel-like, type 1 molecule (a protein strongly expressed in neural tissue, encoding an EGF-like domain) (10–12). Nell-1 is a secreted protein. Structurally, Nell-1 encodes a secretory signal peptide sequence, an $NH_2$-terminal thrombospondin-1–like module, five von Willebrand factor–like repeats with six cysteine residues, and six EGF-like domains. *Nell-1* is also highly conserved across species. For example, 93% amino acid sequence homology exists between rat Nell-1 and human NELL-1.

*Nell-1* encodes a polypeptide with a molecular weight of 90 kDa. When overexpressed in COS cells, the glycosylated form is N-linked to a 50-kDa carbohydrate moiety in eukaryotic cells to generate the 140-kDa form found in the cytoplasm. This 140-kDa protein is further processed to a 130-kDa protein. The Nell-1 protein is secreted as a trimeric form with a high molecular weight (approximately 400 kDa) (13, 14).

Initial studies have suggested that *NELL-1* is preferentially expressed in the craniofacial region of calvarial tissues (12–14). Premature suture closure in CS patients is remarkable for the degree of *NELL-1* overexpression by osteoblast-like cells in osteogenic areas (12). Although *NELL-1* overexpression and premature suture closure may be coincidental findings, our data suggest that *NELL-1* may be a local regulatory factor in cranial suture closure.

In this study, we further verified that *Nell-1* has a role in CS. We created a transgenic mouse model exhibiting generalized *Nell-1* overexpression. *Nell-1* transgenic animals share many of the same features as humans with CS. They demonstrate calvarial overgrowth/overlap and premature suture closure. Infection of osteoblasts with *Nell-1* adenoviral constructs showed that *Nell-1* promotes and accelerates differentiation in osteoblast lineage cells. In addition, Nell-1 downregulation inhibited osteoblast differentiation. *Nell-1*, therefore, represents a candidate gene for producing cranial suture closure and provides new insights in the study of CS and craniofacial development.

## Methods

*Preparation of transgenic mice overexpressing Nell-1.* Rat *Nell-1* cDNA was subcloned from pTM-70 (13, 14) into pCDNA1.1 (Invitrogen, Carlsbad, California, USA), which uses a CMV promoter and an SV40 polyadenylation site. The recombinant plasmid was first transfected into MC3T3 cells (a mouse calvarial cell line) to verify proper protein expression (data not shown). The 4.76-kb DNA fragment containing the CMV promoter, *Nell-1* cDNA, and the SV40 polyadenylation site was then used for microinjection of oocytes. B6C3 mice were used to generate transgenic mice using standard protocols (15). The founders were mated with their nontransgenic littermates to set up transgenic lines.

*Analysis of transgene copy number.* Transgene copy numbers were estimated by PCR and Southern blot analysis. The PCR protocol of establishing transgene copy number was obtained at http://www.med.umich.edu/tamc/spike.html (16). The mass of transgene DNA per 5 μg genomic DNA was calculated as N bp transgene DNA/$3 \times 10^9$ genomic DNA, based on the assumption that the haploid content of a mammalian genome is $3 \times 10^9$ bp and that it takes 10 μg DNA to spike. The size of the insert is 4.76 kb, and the one-copy standard is 7.933 pg per 10 μg genomic DNA. Thirty cycles of PCR were performed and products were separated on electrophoresis gels with ethidium bromide. The intensities were calculated using Eagle Eye II (Stratagene, La Jolla, California, USA).

*Immunohistochemistry.* Detailed preparation of Nell-1 antibody has been documented by Kuroda et al. (13, 14). The antibody recognizes the COOH-terminal region of Nell-1 (CSVDLECIENN). The specificity of the antibody was confirmed by Western blot using protein extracted from *Nell-1*–transfected NIH3T3 cells. A standard avidin-biotin complex/immunoperoxidase protocol (Vector Elite Kit; Vector Laboratories Inc., Burlingame, California, USA) was used with 1:100 Nell-1 antibody dilution. Diaminobenzidine peroxidase substrate and 3-amino-9-ethylcarbazole were used for visualization, and sections were counterstained with hematoxylin.

*Magnetic resonance imaging.* Magnetic resonance imaging (MRI) was performed on formalin-preserved specimens using a Bruker Biospec MR imager (Bruker BioSpin GmbH, Rheinstetten, Germany) with a 7.0-T, 18-cm clear-bore magnet equipped with a microimaging gradient set and a 35-mm internal diameter birdcage radiofrequency coil. Transaxial and sagittal images of the brain and calvarium were obtained using a gradient echo filtered imaging steady-state pulse sequence

with the following parameters: TR/TE, 229.3/64.1 ms; flip angle, 30°; field of view, 2.3 cm; matrix, 256 × 256; slice thickness, 1 mm; and number of excitations, 8. In-plane spatial resolution was approximately 90 μm.

*Microcomputerized tomography scan*. All the data were collected at 30 kVp and 750 mA. The data was reconstructed using the cone-beam algorithm supplied with the MicroCat scanner (Oak Ridge National Laboratory, Oak Ridge, Tennessee, USA). The matrix was 256 × 256 × 256, yielding an isotropic resolution of 140 μm. The quantitative procedures involve the placement of bone phantoms (long rods in the images) containing 0, 50, 250, and 750 mg/cc hydroxyapatite. Visualization of the data was performed using MetaMorph (two dimensional) (Universal Imaging Corp., West Chester, Pennsylvania, USA) and Amira (three dimensional) (Indeed – Visual Concepts GmbH, Berlin, Germany).

*In vivo proliferation analysis*. Newborn mice were injected with BrdU at 100 μg/g. Animals were sacrificed 2 hours after injection. The animals were fixed and immunostained with BrdU antibodies (Sigma-Aldrich, St. Louis, Missouri, USA). Calvarial sutures, brain, and tibiae from transgenic animals and their normal littermates were compared.

*Recombinant defective adenovirus vectors harboring Nell-1 (AdNell-1) and antisense Nell-1 (AdAntiNell-1)*. Rat Nell-1 cDNA was inserted bidirectionally between the human CMV IE1 promoter and the SV40 splice/polyadenylation site flanked by nucleotide sequences from 1 to 454 and from 3,334 to 6,231 of the Ad5 virus. The resulting plasmid, pAdCMV-*Nell-1*, transcribes *Nell-1* leftward relative to the standard Ad5 map. The recombinant adenovirus (Ad) (Ad*Nell-1*) were isolated by cotransfecting 293 cells with pAdCMV-*Nell-1* and pJM17 (Microbix Biosystems Inc., Toronto, Canada), resulting in vectors defective in the *E1-A* viral gene. Clones of recombinant virus were plaque purified and confirmed by Southern blot analysis. Both Ad*Nell-1* and Ad*LacZ* were grown to a high titer and purified once through a CsCl cushion and again on a continuous CsCl gradient. The resulting stocks were $5 \times 10^9$ pfu/ml as assayed by plaque formation on 293 cells. Northern and Western blots were performed to assure the incorporation and expression of the *Nell-1* gene and its protein product.

*Rat calvarial primary cell cultures (FRCCs)*. The isolation of osteogenic cells from embryonic day 18 (E18) rat calvaria was performed as previously described (12). The cells collected from digestions four, five, and six were pooled and plated at $2.5 \times 10^4/cm^2$. Cells within passage two were used.

*Adenoviral infection of osteoblasts*. In order to observe the effects of overexpressing Nell-1, osteoblasts from different lineages were grown to 80% confluence in six-well plates. The media was aspirated and an infective dose (20 pfu/cell in 1 ml serum-free medium) was added to the cultures. Five sets of Ad*Nell-1*, AdAnti*Nell-1,* and control Ad carrying β-Galactosidase (Adβ-Gal) were used. On days 12, 15, and 21 after infection, von Kossa staining was performed. The percentage of area mineralized was analyzed using the Image-Pro Plus system (Media Cybernetics, Silver Spring, Maryland, USA). Comparisons between mice were made using the Student *t* test.

In order to observe the effects of downregulating Nell-1, AdAnti*Nell-1* was added to fetal rat calvarial cell (FRCC) cultures as described above.

*Microarray analysis*. Microarrays were performed using RNA from Ad*Nell-1*– and Ad*β-Gal*–infected MC3T3 cells at 6, 9, and 12 days after infection. I. Nishimura and the University of California Los Angeles Microarrays Core Facility staff have developed bone-related microarrays. The microarrays contain over 37 genes with more than ten internal control genes. Confirmed markers include the following: bone matrix proteins (osteopontin, osteonectin, osteocalcin, bone sialoprotein); receptors ($\alpha_2$-integrin, vitamin D receptor, parathyroid receptor, estrogen receptor); osteoblastic markers (alkaline phosphatase, Cbfa1); adhesive proteins (fibronectin, chondroitin sulfate proteoglycan 1, decorin, tenascin, syndecan, laminin); metalloproteinases (matrix metalloproteinases 1 and 2); growth factors (Bmp2, Bmp7); fibrillar collagens (collagens 1A1, 1A2, 3A1, 5A2, and 11A1); other collagens (collagens 4A1, 6A1, 7A1, 10A1, and 15A1); and fibril-associated collagen with interrupted triple helices (FACITs) (collagens 9A1, 9A2, 12, 14, 16, and 19).

RNA (30 μg total RNA for Cy3 and 60 μg for Cy5) was labeled with random hexamer primers and Cy3- or Cy5-dUTP. The reverse transcriptase–labeled probes were hybridized onto the arrays. Multiple laser scans were performed with a 418 Array Scanner (Affymetrix Inc., Santa Clara, California, USA) to provide mean readouts and standard deviations to verify the reproducibility of the measurements. An average of all the internal controls was calculated and used to normalize hybridization intensities using the IPLab version 3.2 MicroArray suite (Scanalytics Inc., Fairfax, Virginia, USA). The correlation of all osteoblastic markers as a group was calculated and compared between the Ad*Nell-1*–infected cells and the Ad*β-Gal*–infected control cells.

*RT-PCR*. DNase-treated total RNA was used. After initial verification of gene fragment expression through high-cycle PCR, another low-cycle PCR was performed to quantify relative gene expression (12). For each candidate molecule, we determined the cycle number most likely to fall within the linear amplification range by successively reducing the number of cycles (range, 15–35 cycles). Electrophoreses were performed and hybridized with sequence-specific probes labeled wit P32. A PhosphorImager (Molecular Dynamics, Sunnyvale, California, USA) was used to measure the intensities. For each sample, the densitometry value was divided by the *Gapdh* value (performed at 20 cycles) and normalized. Primer sequences were as follows. *Msx2*: forward, 5′-CCTCGGTCAAGTCGGAAAATTC-3′; reverse, 5′-TGGACAGGTACTGTTTCTGGCG-3′; probe, 5′-GAGCACCGTGGATACAGGAG-3′ (annealing temperature, 68°C). *Cbfa1*: forward, 5′-CTGTGTGGCTCCTAACAAGTGTG-3′; reverse, 5′-GGATTCTGGCAATCACAAGCTGTC-3′; probe, 5′-CCTACTCACTGTCCGGGGAGTCCTGC-3′

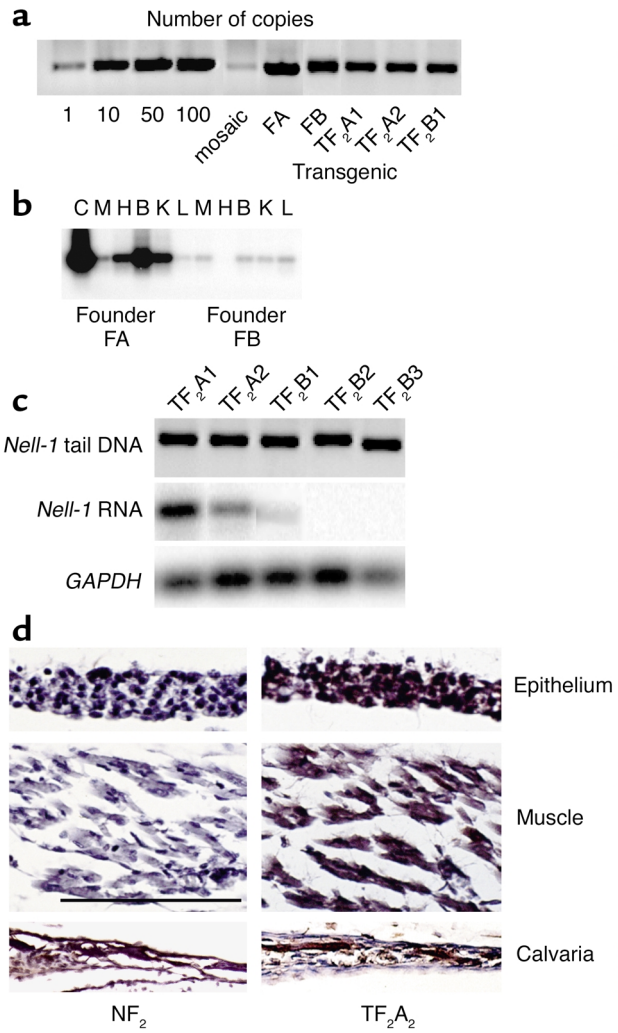


**Figure 1**

*Nell-1* transgenic mice compared with nontransgenic littermates. (**a**) Transgene copy number. The founders (FA and FB) and their progeny ($TF_2A1$, $TF_2A2$, and $TF_2B1$) have copy numbers between 50 and 100. $TF_2A1$ and $TF_2A2$ are from the founder A line. $TF_2B1$, $TF_2B2$, and $TF_2B3$ are from the founder B line. (**b**) RT-PCR analyses of *Nell-1* RNA expression in both founders. C, control *Nell-1* plasmid; M, muscle; H, heart; B, bone; K, kidney; L, liver. (**c**) Whole body (without head) RNA of newborn progeny. $TF_2A1$ and $TF_2A2$ express different levels of *Nell-1*. $TF_2B1$ expresses *Nell-1* weakly, while $TF_2B2$ and $TF_2B3$ have no *Nell-1* expression. (**d**) Left panels, immunolocalization of Nell-1 protein in newborn $NF_2$ epithelium, muscle, and calvarial bone. There is no detectable Nell-1 expression (brown staining indicates the presence of Nell-1) except some staining in the calvarial bone. Right panels, immunolocalization of Nell-1 protein in $TF_2A2$ epithelium, muscle, and calvarial bone. Abundant Nell-1 expression is present throughout all soft tissue layers as well as in bone. Bar represents 50 μm.

(annealing temperature, 66°C). Osteocalcin: forward, 5′-ATGAGGACCCTCTCTCTGCTC-3′; reverse, 5′-GTGGTGCCATAGATGCGCTTG-3′; probe CATGTCAAGCAGGGAGGGCA-3′ (annealing temperature, 66°C). Osteopontin: forward, 5′-AGCAGGAATACTAACTGC-3′; reverse, 5′-GATTATAGTGACACAGAC-3′; probe 5′-GCCCTGAGCTTAGTTCGTTG-3′ (annealing temperature, 66°C). *Nell-1*: (12).

*Flow cytometry analysis*. Cells were seeded on 60-mm plates at $5 \times 10^5$ cells/plate. Cells were harvested at 24, 36, 48, and 72 hours after infection with Ad*Nell-1* and Ad*β-Gal*. One million cells were used for flow cytometry, and this procedure was repeated three times. Hypotonic DNA staining buffer containing propidium iodide was added to the cells for flow cytometry.

## Results

*Construction of CMV promoter/Nell-1 transgenic mice*. To investigate the effects of generalized *Nell-1* overexpression in vivo, transgenic mice in which *Nell-1* is expressed under the control of the CMV promoter were produced. Copy number was confirmed by Southern blot and PCR (Figure 1a). RNA analysis (Figure 1b) and immunohistochemistry (data not shown) further confirmed expression of Nell-1 in founders. *Nell-1*–overexpressing founders were crossed with nontransgenic littermates, and comprehensive analyses were conducted on $F_2$ progeny. Because most human CS phenotypes are readily apparent in newborns, 42 newborn mice, representing six litters from two lines, were examined. The morphology of these mice was assessed for developmental anomalies, including suture closure. The mice were subsequently genotyped. Suture patency was determined by the absence (indicating suture closure) or the presence (indicating suture patency) of visible blood vessels underneath the suture. Suture closure was further confirmed under a dissecting microscope. Two of the six litters examined, representing 20 progeny, did not yield any newborns with obvious craniofacial defects and were *Nell-1* transgene negative. These litters were not examined further. Progeny with craniofacial defects were recovered in each of the four remaining litters. The progeny of these four litters (22 mice) were analyzed further. A limitation of this rapid screening method is that mild CS with only focal points of suture closure may not be detected, and therefore *Nell-1* overexpression might appear to have lower penetrance.

Thirteen (60%) of the 22 newborn progeny were transgenic, with gene copy numbers similar to the founder *Nell-1* mice (prediction is 50%). *Nell-1* RNA levels of the 13 *Nell-1* DNA–positive transgenic $F_2$ ($TF_2$) mice were examined. Eight (62%) were positive for *Nell-1* RNA expression. However, the level of expression varied (Figure 1c). The reason for low or nearly absent *Nell-1* expression in some $TF_2$ mice despite their high transgene copy numbers is not clear, but epigenetic effects such as heterochromatin formation around the inserts may play a significant role in the high variability of transgene expression (17). RNA levels also differed in different tissues isolated from the same litter. Liu et al. also made this observation of variegation when they overexpressed *Msx2* using a *CMV* promoter (5, 6). Therefore transgenic *Nell-1* transcription may not necessarily correlate with gene copy number, and may also vary according to cell type.

To determine whether *Nell-1* overexpression in our transgenic model was physiologically relevant, we compared *Nell-1* RNA expression levels from the whole heads of three $TF_2$ progeny with mild CS phenotypes to levels

in nontransgenic normal littermates ($NF_2$ mice). $TF_2$ mice displayed up to fourfold-increased *Nell-1* expression (data not shown). This was comparable to levels of *NELL-1* overexpression in human CS patients in whom two- to fourfold increases have been observed (12). This suggests that *Nell-1* overexpression levels in our model were clinically relevant rather than superphysiologic.

*Phenotypic analyses of Nell-1 transgenic mice.* Three of the eight *Nell-1* RNA-positive $TF_2$ mice demonstrated severe craniofacial anomalies and died shortly after birth (see Figure 2, a–c, and Figure 4). These mice also demonstrated detectable *Nell-1* transgene expression in their total body mRNA (Figure 1c) that was verified by Nell-1 immunostaining of skin, liver, and calvaria (Figure 1d).

Morphological examination of one of the most severely affected $TF_2$ mice revealed a large protuberance in the paramedial parietal area with completely closed sagittal and posterior-frontal (PF) sutures and partially closed coronal sutures (Figure 2, a–c). Clinically, this is similar to craniotelencephalic dysplasia, a form of human CS with premature sagittal, metopic, and coronal suture closure with secondary frontal bone bossing and paramedial encephalocele (Figure 2d) (1). Brain MRI of this $TF_2$ mouse revealed significantly reduced ventricle size and increased parenchymal edema, both of which are suggestive of increased intracranial pressures (Figure 2e). Continued brain growth in the face of premature suture closure also generates increased intracranial pressures in humans with untreated CS. Microcomputerized tomography (MCT) scan and MRI analysis also demonstrated structural abnormalities in the cranium of this $TF_2$ mouse (Figure 2, f and g).

Histological examination of Nell-1 phenotype-positive $TF_2$ mice revealed distinct differences from $NF_2$ littermates. As in human CS, $TF_2$ mice displayed prematurely closing sutures seen histologically as thickened, disorganized ridges of calvarial ridges with closing/overlapping osteogenic fronts (Figure 3, a and b). Whole-mount skeletal staining did not show any observable extracranial skeletal anomalies. Hematoxylin and eosin and tartrate-resistant acid phosphatase staining of palatal and midmandible sutures, vertebrae, and long bones did not reveal any abnormal histology or increase in osteoclast number. Therefore, the effects of Nell-1 expression appear to be confined to the calvaria. Despite pan-tissue *Nell-1* expression due to the use of the *CMV* promoter, $TF_2$ mice exhibited cranial-specific anomalies that primarily affected calvarial suture patency and closure. Immunohistochemistry showed increased in vivo expression of osteoblastic differentiation markers (Figure 3, c and d).

In situ BrdU analysis of prematurely closing cranial sutures in *Nell-1*–expressing $TF_2$ mice demonstrated significantly reduced numbers of proliferating cells within osteogenic areas along suture edges (Figure 3, e and f). These data suggest that *Nell-1* overexpression is associated with osteoblast differentiation. No statistically significant difference was observed in the total number (Figure 3g) of cells per field along the sutures of $TF_2$ and $NF_2$ mice. The observed decrease in proliferating cells may be secondary to the decreased proliferative abilities of differentiated osteoblasts or may reflect a primary defect in osteoblast proliferation.

Morphologic examination of a second severely affected $TF_2$ animal showed significant cranial suture

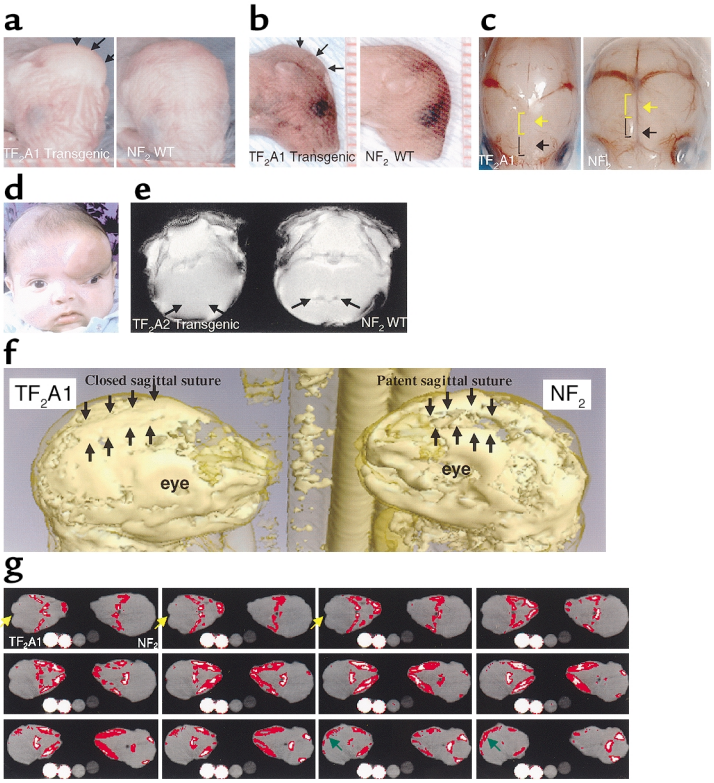


**Figure 2**
Phenotypic evaluation of *Nell-1* transgenic mice. (**a** and **b**) Left panels show a newborn Nell-1 phenotype–positive ($TF_2A1$) mouse. Note the protrusion in the frontoparietal area (arrows). Right panels show an $NF_2$ littermate. (**c**) Left panel, $TF_2A2$ mouse with the scalp removed. The sagittal (yellow arrow) and PF (black arrow) sutures are closed. Right panel, skull of the $NF_2$ littermate with patent sagittal (yellow arrows) and PF (black arrow) sutures and normal vasculature underneath the patent sutures. (**d**) An infant with craniotelencephalic dysplasia, a severe form of CS. (**e**) Brain MRI of $TF_2A1$ mouse (left) and $NF_2$ littermate (right). Note the complete absence of ventricles, suggesting elevated intracranial pressure in the $TF_2A1$ mouse (arrows, left) relative to its $NF_2$ littermate (arrows, right). (**f**) MCT-reconstructed three-dimensional skull views of the newborn Nell-1 phenotype-positive $TF_2A1$ (left) and $NF_2$ (right) littermates. Arrows indicate sagittal and PF suture sites. In $TF_2A1$ mice, the sagittal and PF sutures are largely closed and replaced with an abnormal ridge. In the $NF_2$ littermate, both sagittal and PF sutures are patent. Complete opacity corresponds to greater than 50 mg/cc mineralization. The vertical rods in the background are phantom reference rods corresponding to mineralization densities (from left to right) of 50, 100, 150, and 200 mg/cc. (**g**) Serial axial MCT sections of the $TF_2A1$ (left) and $NF_2$ littermates (right) shown in **f**. Yellow arrows indicate the distortion of the cranium. Green arrows indicate increased mineralization of the calvarium in the $TF_2A$ mouse (arrow, right).

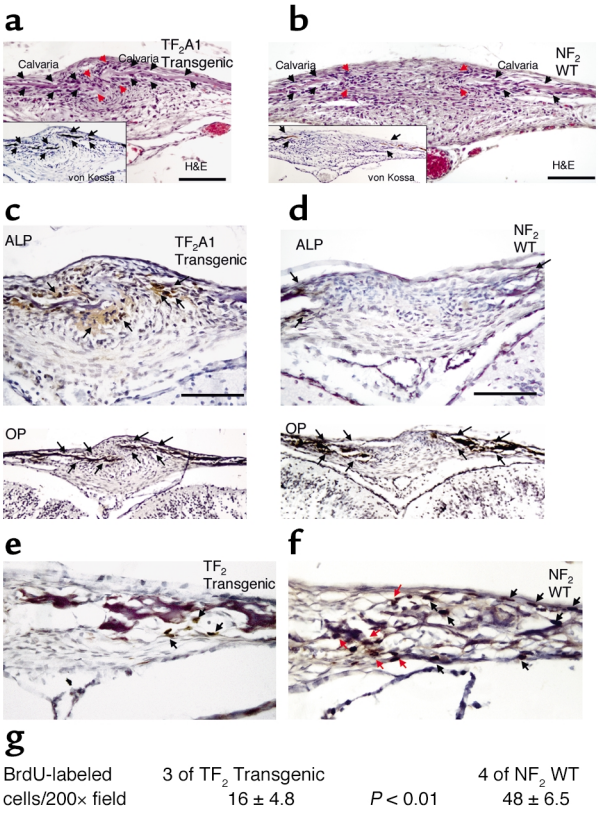


**Figure 3**
Histologic and immunohistologic evaluation of *Nell-1* transgenic mice. (**a**) Hematoxylin and eosin staining of the sagittal suture of a Nell-1 phenotype-positive $TF_2A1$ mouse. There is closure of the suture, shown by the overlap of calvarial edges (black arrows) and closing osteogenic fronts (red arrows). Lower left panel shows von Kossa staining. Note the close proximity of mineralized calvarial edges. (**b**) Hematoxylin and eosin staining of the sagittal suture from an $NF_2$ littermate. Note the large distance separating the two calvarial edges (black arrows) at the patent suture site, as well as the advancing osteogenic fronts (red arrows). Lower left panel shows von Kossa staining. Black color indicates mineralization. (**c**) Immunolocalization of alkaline phosphatase (ALP) in a $TF_2A1$ mouse. Brown staining indicates the presence of alkaline phosphatase (arrows). Lower panel represents the immunolocalization of osteopontin at lower magnification. (**d**) Upper panel shows immunolocalization of alkaline phosphatase in newborn $NF_2$ cranial suture. Lower panel represents the immunolocalization of osteopontin (OP) at a lower magnification. Bar represents 50 μm. (**e**) BrdU staining of a $TF_2$ sagittal suture. The nuclei of proliferating cells are stained brown (black arrows). Proliferating cells are significantly decreased relative to those shown for $NF_2$ in **d**. (**f**) BrdU staining of a newborn $NF_2$ mouse sagittal suture. Numerous brown-stained cells are proliferating along the calvarial edges (black arrows) of the patent suture, as well as along the advancing osteogenic fronts (red arrows). H&E, hematoxylin and eosin. (**g**) Number of proliferating cells per field.

obliteration, primarily in the midline (i.e., sagittal and posterior frontal sutures), with bulging in the occipital (posterior) area. Overall, the skull was narrow and resembled those of humans with scaphocephaly and premature sagittal synostosis. MCT scanning revealed complete PF suture and partial sagittal and coronal suture closure (Figure 4b). Histological correlation revealed marked calvarial bone overgrowth and overlap in the closed area of the sagittal suture (Figure 4b).

To examine $TF_2$ embryologic development during gestation, two litters of E15 $TF_2$ progeny were sacrificed. Nonviable littermates with exencephaly-like phenotypes were observed in two of 19 embryos. Interestingly, Liu et al. reported a similar finding of exencephaly for *Msx2*-overexpressing mice (6). The etiology for this phenotype is not clear. This result may also help to explain the observed low incidence of severely affected $TF_2$ progeny among newborn mice.

*Overexpression of Nell-1 in vitro accelerates osteoblast differentiation*. Dysregulated bone formation has been proposed as a possible mechanism for calvarial overgrowth/overlap and premature suture closure (18). Because abnormal suture site osteogenesis is the cardinal feature of *Nell-1* $TF_2$ mice exhibiting premature suture closure, we hypothesized that *Nell-1* overexpression may alter normal calvarial osteoblast cell cycling and differentiation pathways to promote premature osteogenesis.

To test our hypothesis, we first examined the effect of *Nell-1* on mineralization, a hallmark of osteoblast differentiation in vitro. Primary FRCC and MC3T3 (a mouse calvarial osteoblast-like cell line) cultures were infected with Ad*Nell-1* at 20 pfu/cell in the presence of ascorbic acid. Ascorbic acid is essential for the induction and terminal differentiation/mineralization of osteoblasts (19). Ad*Nell-1*–infected FRCC and MC3T3 cultures mineralized more rapidly and profusely (more than sixfold) than Ad*β-Gal*–infected controls did (Figure 5, a and b). In contrast, Ad*Nell-1* infection did not elicit any mineralization response in NIH3T3, adult, or fetal rat primary fibroblast cells (data not shown). These data suggest that *Nell-1* accelerates osteoblast mineralization and that the effects are osteoblast-specific.

Our previous in vivo BrdU results demonstrated significantly reduced cell proliferation along the osteogenic front in $TF_2$ mice. To determine whether *Nell-1* overexpression in vitro also affects cell cycling, Ad*Nell-1*–infected MC3T3 cells (and Ad*β-Gal* controls, with and without ascorbic acid treatment and with and without 24 hours of serum starvation) were examined by flow cytometry at 24 and 48 hours after infection. No statistically significant changes were observed in populations in different phases of the cell cycle (two-tailed Student *t* test, $P > 0.05$). The fact that MC3T3 cells did not demonstrate decreased proliferation after *Nell-1* transfection may reflect inherent differences between in vivo and in vitro osteoblast cells or the influence of the extracellular milieu and stage of cellular differentiation.

Normal in vitro osteoblast differentiation is heralded by nodule formation (osteoblast cell aggregates) followed by mineralization. This differentiation program requires ascorbic acid. Interestingly, Ad*Nell-1*–infected MC3T3 cells, when cultured *without* ascorbic acid, also formed nodules expressing alkaline phosphatase beginning on day 3 after infection; control Ad*β-Gal*–infected cells did not. *Nell-1*–induced nodules in the absence of

ascorbic acid, however, were smaller (≤ 20 cells per nodule, detectable at 100× magnification), and did not reveal mineralization with von Kossa staining (Figure 5c). Moreover, late differentiation markers such as osteopontin were not expressed in these "micronodules." The formation of micronodules by Ad*Nell-1*–infected osteoblasts in the absence of ascorbic acid suggests that *Nell-1* alone may influence cell-cell adhesion but is not sufficient to induce full osteoblast differentiation.

To prove that *Nell-1* enhances osteoblast differentiation, RNA from Ad*Nell-1*–infected MC3T3 cells, cultured under normal conditions with ascorbic acid, were subjected to microarray analyses of various bone-specific markers at 6, 9, and 12 days after infection (Figure 5, d–f). The purpose of the microarray was to determine whether Ad*Nell-1*–infected and control Ad*β-Gal*–infected cells demonstrated distinct differences in overall osteoblast differentiation marker expression patterns using regression analysis. By day 12, the expression pattern of osteoblast differentiation markers was distinctly different between Ad*Nell-1*– infected cells and Ad*β-Gal*–infected cells ($r^2$ = 0.334). Microarray analyses used in this experiment were not meant to quantitate the expression of individual genes. Individual gene expression patterns should be interpreted with caution, e.g., genes with two or more fold up or downregulation should then be analyzed. Results should also be confirmed with RT-PCR or RNA analyses. Late differentiation markers, such as Bmp7, osteopontin, and osteocalcin, were upregulated more than twofold in Ad*Nell-1*–infected cells, while earlier markers, such as type I collagen and osteonectin, were downregulated more than twofold (Figure 5g). This suggests that *Nell-1* promotes osteoblast differentiation. Osteocalcin and osteopontin RNA upregulation were verified by RNA electrophoresis (see Figure 6, c and d). Neither microarray nor reduced-cycle RT-PCR analyses demonstrated any significant changes in expression of *Cbfa1*, *Tgf-β1, -β2, and -β3,* or *Tgf-β types -I, -II,* and *-III* receptors, *Fgfr1*, or *Fgfr2* in Ad*Nell-1*–infected MC3T3 cells (data not shown). This suggests that *Nell-1* may operate downstream of these candidate genes or may affect distinctly different pathways.

*Downregulation of Nell-1 in vitro delays osteoblast differentiation*. To further address the physiologic function of Nell-1 in osteoblast differentiation, we tested the effect of downregulating the Nell-1 protein through adenoviral antisense *Nell-1* infection in osteoblasts. FRCC cultures were infected with AdAnti*Nell-1* at 20 pfu/cell in the presence of ascorbic acid. AdAnti*Nell-1* downregulated Nell-1 protein expression to 40% of its normal expression level (Figure 6a). FRCC cultures expressed significantly less alkaline phosphatase than did Ad*β-Gal*–infected controls or Ad*Nell-1*–infected cells (Figure 6b). Osteocalcin and osteopontin RNA expression was also downregulated in AdAnti*Nell-1* cells (Figure 6, c and d). The ratio of osteocalcin in AdAnti*Nell-1*–infected cells to osteocalcin in Ad*β-Gal* controls was less than 1:4 on day 9 and 1:2 on day 12 by Northern analysis. The ratio of osteopontin in AdAnti*Nell-1*–infected cells to that in Ad*β-Gal* controls was less than 1:5 on days 6 and 9, and less than 2:5 on day 12. Therefore, knockdown data complement the overexpression data and suggest that *Nell-1* plays an important role in osteoblast differentiation.

## Discussion

NELL-1 is a relatively newly discovered molecule with unknown function. Because of the observed transient upregulation of *NELL-1* during premature suture closure in CS patients (12), we simulated *NELL-1* overexpression in a mouse model in order to investigate novel potential functions of *Nell-1* in craniofacial development and pathology. We observed early suture closure and increased osteoblast differentiation in *Nell-1* transgenic mice. Therefore, *Nell-1* is likely a candidate for the control of local suture closure, and the overexpression of *Nell-1* may play an important role in the mechanism of premature suture closure in CS. Based on our overexpression and knockdown in vitro data, *Nell-1* most likely influences osteoblast differentiation. However, the molecular mechanism is unknown.

Nell-1 may induce osteoblast differentiation by binding and then sequestering or activating ligands, as well as by triggering receptor-mediated signaling (20). Nell-1's combination of chordin-like, cysteine-rich domains,

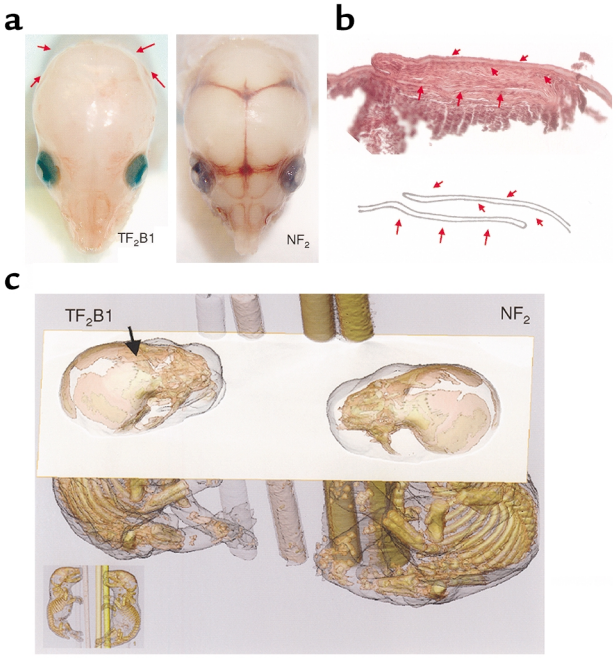


**Figure 4**
*Nell-1* transgenic $TF_2B1$ mouse compared with a nontransgenic littermate. (**a**) Left, newborn $TF_2B1$ mouse with the scalp removed. Note the abnormal bulging of the occipital area and the relatively narrow width of the cranium. Right, an $NF_2$ littermate. In the $TF_2B1$ transgenic animal, the sagittal suture and several other sutures are closed. (**b**) Hematoxylin and eosin staining of $TF_2B1$ sagittal suture. Premature closure of the suture is manifest in the severe overlap of calvarial edges (red arrows). The underlying brain tissue has been removed for RNA analysis. (**c**) Three-dimensional MCT reconstruction of a $TF_2B1$ mouse (left) and its $NF_2$ littermate (right). Note the area of premature midline suture closure in the $TF_2B1$ mouse (arrow, left).

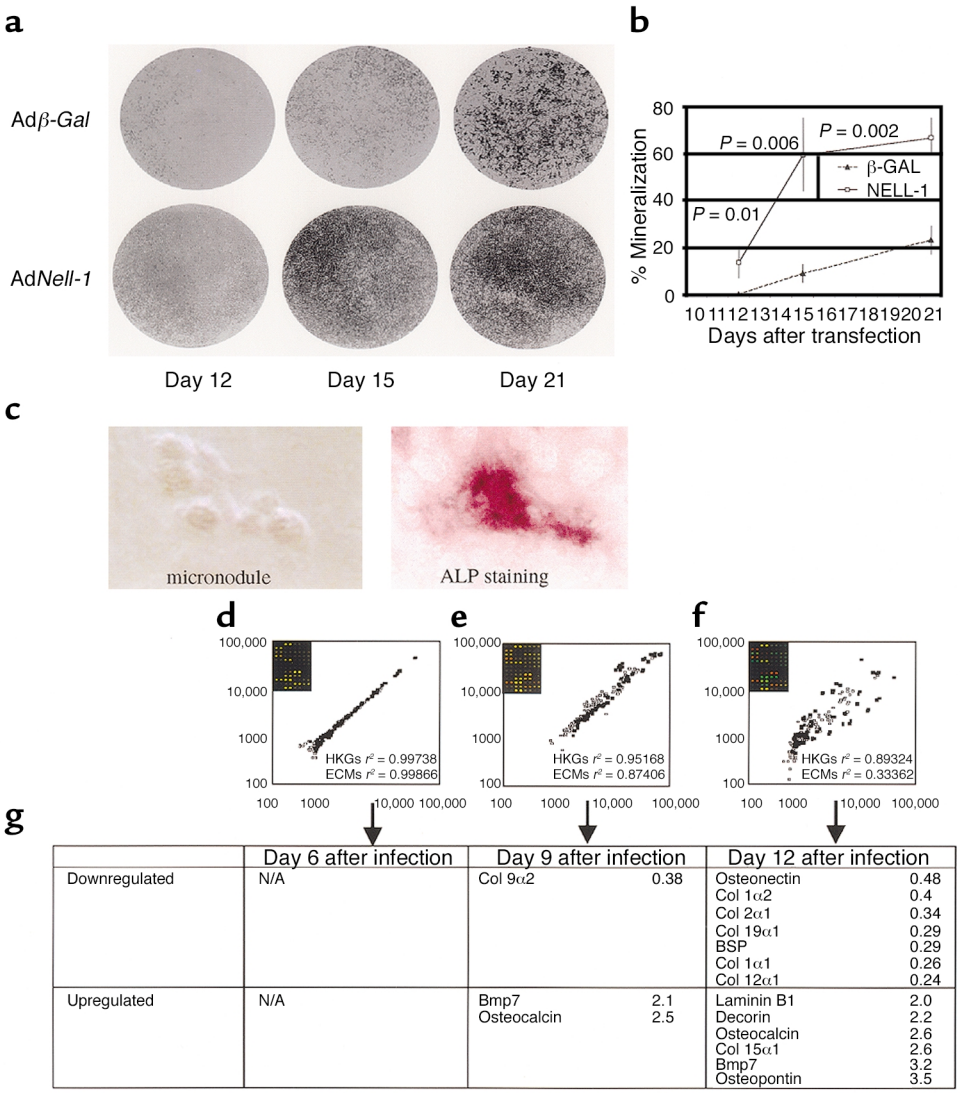


| | Day 6 after infection | Day 9 after infection | | Day 12 after infection | |
|---|---|---|---|---|---|
| Downregulated | N/A | Col 9α2 | 0.38 | Osteonectin | 0.48 |
| | | | | Col 1α2 | 0.4 |
| | | | | Col 2α1 | 0.34 |
| | | | | Col 19α1 | 0.29 |
| | | | | BSP | 0.29 |
| | | | | Col 1α1 | 0.26 |
| | | | | Col 12α1 | 0.24 |
| Upregulated | N/A | Bmp7 | 2.1 | Laminin B1 | 2.0 |
| | | Osteocalcin | 2.5 | Decorin | 2.2 |
| | | | | Osteocalcin | 2.6 |
| | | | | Col 15α1 | 2.6 |
| | | | | Bmp7 | 3.2 |
| | | | | Osteopontin | 3.5 |

**Figure 5**
Effects of *Nell-1* overexpression on mineralization and bone marker expression. (**a**) FRCC culture infected with 20 pfu/cell Ad*Nell-1*, stained with von Kossa stain. Control cell cultures were infected with Ad*β-Gal*. Experiments were performed in triplicate. Mineralized nodules are stained black. (**b**) Quantitation and statistical analysis of mineralized areas. Ad*Nell-1*–infected cultures demonstrated significantly greater mineralization than did Ad*β-Gal* controls. (**c**) Ad*Nell-1*–infected MC3T3 cells grown without ascorbic acid. Typical micronodule appearance is shown. Right panel represents alkaline phosphatase staining of a micronodule. (**d**–**f**) Microarrays of Ad*Nell*–infected MC3T3 cells on postinfection days 6, 9, and 12, respectively. Gene expression intensities have been normalized using standardized housekeeping genes (HKGs). Hybridization intensities of Ad*Nell-1*–infected cells are represented on the *y* axis. Hybridization intensities of Ad*β-Gal*–infected cells are represented on the *x* axis. HKGs $r^2$ represents the correlation of housekeeping genes (filled squares) between the two samples. ECMs $r^2$ represents the correlation of candidate gene expression (open squares) between the two samples. A photograph of the microarray reading is attached in the upper left corner of each diagram. A twofold or greater upregulation is represented in red, while a twofold or greater downregulation is represented in green (**g**) Table summarizing genes with a difference in expression that is twofold higher or lower after Ad*Nell-1* infection. The ratio is calculated as *Nell-1*/*β-Gal*. Col, collagen.

$NH_2$-terminal thrombospondin–like module, and EGF-like repeats make it a likely modulator of growth factor activity. We have conducted preliminary studies to test this possibility. To determine whether Nell-1 binds to known EGF-like receptors, we previously added Nell-1 to IL-3–dependent cells expressing ErbB1, -2, -3, or -4. The addition of Nell-1 failed to produce tyrosine phosphorylation of these receptors. Nell-1, therefore, is not a ligand for these receptors even though Nell-1 is a known secretory protein with EGF-like repeats (13). Instead, Nell-1 may interact with other specific receptors that may be expressed only by certain cell types. Using the yeast two-hybrid system (14), we are in the process of isolating potential Nell-1 receptors, although no such receptors have been found yet. Because Nell-1 shares many motifs with thrombospondin-1 and chordin, it may hypothetically activate or sequester members of the TGF-β superfamily and function as a thrombospondin-1–like

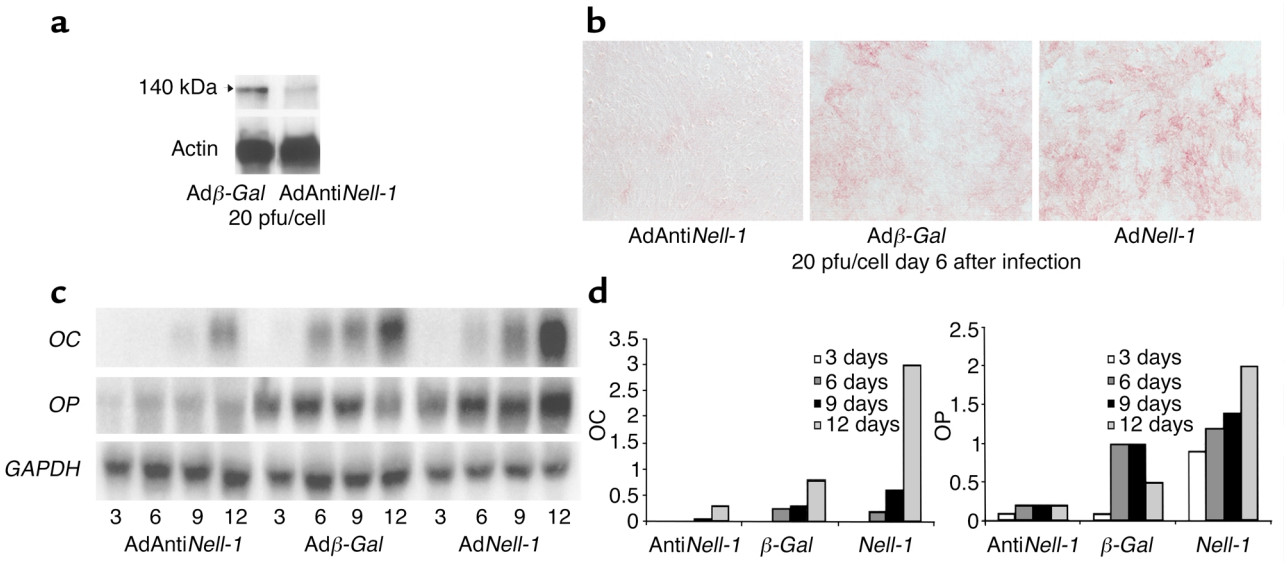


**Figure 6**
Effect of Nell-1 downregulation on alkaline phosphatase expression and bone marker expression. (**a**) Western blot analysis of Nell-1 protein expression in rat FRCCs infected with 20 pfu/cell AdAnti*Nell-1* or Ad*β-Gal* control. Downregulation of approximately 60% is observed. (**b**) Alkaline phosphatase staining (in red) of FRCCs. AdAnti*Nell-1*–infected cells have significantly less staining than do control and Ad*Nell-1*–infected cells. (**c**) Northern analyses of FRCCs on days 3, 6, 9, and 12 after infection. AdAnti*Nell-1*–infected cells have significantly less osteocalcin and osteopontin expression. (**d**) Expression of osteocalcin (OC) and osteopontin (OP) measured by PhosphorImager and normalized by *GAPDH*.

molecule to facilitate latent TGF-β1 activation (21). Recently, Abreu et al. suggested that Nell-1 is a member of the "chordin-like cysteine-rich domains" family, which includes chordin, kielin, crossveinless, twisted gastrulation (Tsg), and connective TGF (20). A common feature of the chordin-like cysteine-rich domains family members is that their expression is temporally and spatially specific, particularly in patterning. Another common feature is their interaction with members of the Bmp family and subsequent function as pro- or anti-Bmp's.

*Specific expression and function of Nell-1 in vivo*. In our previous studies, we reported the earliest detectable *Nell-1* expression in E11–E14 mice (12). *Nell-1* is preferentially expressed in the craniofacial region, both prenatally and postnatally, during growth and development. Immunohistochemistry showed that Nell-1 localizes primarily to bone-forming areas of sutures and the calvarium and ossifying membranous bone in the mandible (data not shown). Both calvarial and mandibular membranous bones are thought to be neural crest derivatives (22). Preferential *Nell-1* expression in the craniofacial region by neural crest derivatives suggests that Nell-1 may be important during skeletal craniofacial growth and development.

Surprisingly, unlike other CS models involving generalized gene overexpression, *Nell-1* transgenic mice displayed anomalies that were restricted to the calvarial bone, despite generalized, non-tissue-specific *Nell-1* overexpression. This further supports our hypothesis that Nell-1 undergoes highly specific interaction to induce osteoblast differentiation. *Nell-1* overexpression, therefore, is less likely to cause suture closure by nonspecifically perturbing the function of homologous molecules such as thrombospondin-1. This was verified by knockdown studies in vitro.

*Effect of Nell-1 on osteoblast differentiation*. Normal osteoblasts cultured without ascorbic acid do not differentiate. Osteoblasts overexpressing *Nell-1*, on the other hand, form micronodules and express alkaline phosphatase in the absence of ascorbic acid. This suggests that *Nell-1* alone is sufficient to induce some degree of osteoblast differentiation.

In addition, RNA microarray analyses of *Nell-1* overexpression in osteoblasts cultured under normal conditions (i.e., with ascorbic acid) demonstrated upregulation of late differentiation markers at day 12 after transfection. Ad*Nell-1*–transfected osteoblasts also exhibited increased mineralization beginning on day 12 after transfection. These data indicate that *Nell-1* may accelerate the rate of calvarial osteoblast differentiation and mineralization.

*Nell-1* overexpression may not reflect the true physiological function of Nell-1, but rather the effect of *Nell-1* overexpression on other thrombospondin-like molecules. Downregulation of *Nell-1* clearly inhibited osteoblast differentiation. Nell-1 is therefore likely to

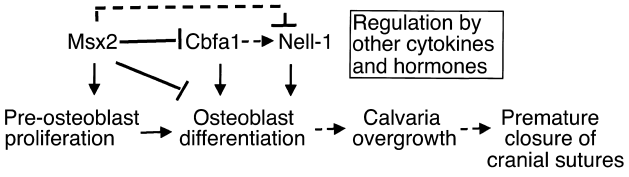


**Figure 7**
Hypothetical model of *Nell-1* function in premature suture closure. Dashed line represents potential modulation.

be both sufficient and required for osteoblast differentiation in vitro. However, *Nell-1* null mice need to be produced in order to justify this conclusion in vivo.

*Nell-1's relation to currently known CS models*. *Nell-1* overexpression produces craniofacial abnormalities similar to those resulting from *Msx2* overexpression in vivo. Both mouse models exhibit suture overgrowth and an increased incidence of exencephaly. However, the cellular functions of these two genes appear to be distinctly different; continuous *Msx2* overexpression induces proliferation and inhibits differentiation, while *Nell-1* enhances differentiation. Mice with a $Pro^{250} \rightarrow Arg$ mutation in *Fgfr1*, which induces *Cbfa1* overexpression, have distinctly different phenotypes from mice overexpressing *Nell-1* because calvarial fusion occurs much later (postnatal days 16–21) and gross suture overlap does not occur (8) in the mice with the $Pro^{250}$ mutation. However, *Cbfa1* has a similar cellular function to *Nell-1* in vitro; both induce osteoblast differentiation with upregulation of bone marker genes. *Nell-1* expression is modulated by *Msx2* and *Cbfa1*. *Cbfa1* transfection of FRCCs upregulated *Nell-1* expression within 24 hours, while *Msx2* transfection and *Cbfa1/Msx2* cotransfection downregulated *Nell-1* expression (unpublished observations). While all these candidate genes are important to the understanding of CS, *Msx2* may be important in the earlier stages of CS (5, 6), while *Fgfr1/Cbfa1* may play a role in the later stages of suture closure. Future investigation of the *Nell-1* promoter, which contains conserved Cbfa1 and Msx binding sequences, may provide further understanding of their interactions (Figure 7). These observations underscore the complexity of the dynamic genetic and environmental interactions in craniofacial growth and development.

In conclusion, we have created an animal model of human nonsyndromic CS by overexpressing *Nell-1*. Unlike other available CS models involving mutations in *FGFRs* or homeobox genes (1, 2, 8), our animal model exhibited anomalies that were localized to the craniofacial skeleton. We hypothesize that *Nell-1* is sufficient, and probably required, to promote and accelerate calvarial osteoblast differentiation and bone formation. Mechanistically, *Nell-1* overexpression induces intramembranous bone formation in cranial sutures and may lead to calvarial overgrowth/overlap and subsequent premature suture closure.

Although *Nell-1* has not yet been identified as a cause of CS in human genetic studies, the data strongly suggest that Nell-1 is part of a complex chain of events resulting in premature suture closure (1). The resemblance of *Nell-1* transgenic mice to humans with nonsyndromic CS and *Nell-1*'s association with known CS candidate genes provides new insights for CS research. Further investigation of the regulation and mechanism of *Nell-1* in suture closure and bone formation can potentially accelerate our understanding of the cascade of events leading to premature suture closure in CS.


## Acknowledgments

We thank Frank Netter, Ernie Kwong, and Hao Fu Lee for assistance with graphics. We thank Sharon Hunt and Karen Lyons for editing the manuscript. We thank Robert Maxson, M. Luisa Truela-Arispe, and E.M. DeRobertis for their input. This research is supported by the Wunderman Family Foundation, the Oral and Maxillofacial Surgery Foundation, the NIH and University of California, Los Angeles, Clinical Research Center, the National Institute of Dental and Craniofacial Research (K23DE00423), and the American Association of Orthodontists Foundation.



1. Cohen, M.M, Jr., and MacLean, R.E. 2000. *Craniosynostosis: diagnosis, evaluation and management.* 2nd edition. Oxford University Press. New York, New York, USA. 454 pp.
2. Coffin, J.D., et al. 1995. Abnormal bone growth and selective translational regulation in basic fibroblast growth factor (FGF-2) transgenic mice. *Mol. Biol. Cell*. **6**:1861–1873.
3. Carlton, M.B., Colledge, W.H., and Evans, M.J. 1998. Crouzon-like craniofacial dysmorphology in the mouse is caused by an insertional mutation at the Fgf3/Fgf4 locus. *Dev. Dyn*. **212**:242–249.
4. Jabs, E.W., et al. 1993. A mutation in the homeodomain of the human MSX2 gene in a family affected with autosomal dominant craniosynostosis. *Cell*. **75**:443–450.
5. Liu, Y.H., et al. 1995. Premature suture closure and ectopic cranial bone in mice expressing Msx2 transgenes in the developing skull. *Proc. Natl. Acad. Sci. USA*. **92**:6137–6141.
6. Liu, Y.H., et al. 1999. Msx2 gene dosage influences the number of proliferative osteogenic cells in growth centers of the developing murine skull: a possible mechanism for MSX2-mediated craniosynostosis in humans. *Dev. Biol*. **205**:260–274.
7. Ma, L., Golden, S., Wu, L., and Maxson, R. 1996. The molecular basis of Boston-type craniosynostosis: the Pro148→His mutation in the N-terminal arm of the MSX2 homeodomain stabilizes DNA binding without altering nucleotide sequence preferences. *Hum. Mol. Genet*. **5**:1915–1920.
8. Zhou, Y.X., et al. 2000. A Pro250Arg substitution in mouse Fgfr1 causes increased expression of Cbfa1 and premature fusion of calvarial sutures. *Hum. Mol. Genet*. **9**:2001–2008.
9. Otto, F., Kanegane, H., and Mundlos, S. 2002. Mutations in the RUNX2 gene in patients with cleidocranial dysplasia. *Hum. Mutat*. **19**:209–216.
10. Matsuhashi, S., et al. 1996. New gene, nel, encoding a Mr 91 K protein with EGF-like repeats is strongly expressed in neural tissues of early stage chick embryos [erratum 1996, **207**:233–234]. *Dev. Dyn*. **203**:212–222.
11. Watanabe, T.K., et al. 1996. Cloning and characterization of two novel human cDNAs (NELL1 and NELL2) encoding proteins with six EGF-like repeats. *Genomics*. **38**:273–276.
12. Ting, K., et al. 1999. Human NELL-1 expressed in unilateral coronal synostosis. *J. Bone Miner. Res*. **14**:80–89.
13. Kuroda, S., and Tanizawa, K. 1999. Involvement of epidermal growth factor-like domain of NELL proteins in the novel protein-protein interaction with protein kinase C. *Biochem. Biophys. Res. Commun*. **265**:752–757.
14. Kuroda, S., et al. 1999. Biochemical characterization and expression analysis of neural thrombospondin-1-like proteins NELL1 and NELL2. *Biochem. Biophys. Res. Commun*. **265**:79–86.
15. Hogan, B.C., Beddington, R., Constantini, F., and Lacy, E. 1986. Manipulating the mouse embryo: a laboratory manual. Cold Springs Harbor Laboratory Press. Cold Springs Harbor, New York, USA. 332 pp.
16. Laird, P.W., et al. 1991. Simplified mammalian DNA isolation procedure. *Nucleic Acids Res*. **19**:4293.
17. Palmiter, R.D., Wilkie, T.M., Chen, H.Y., and Brinster, R.L. 1984. Transmission distortion and mosaicism in an unusual transgenic mouse pedigree. *Cell*. **36**:869–877.
18. Kim, H.J., Rice, D.P., Kettunen, P.J., and Thesleff, I. 1998. FGF-, BMP- and Shh-mediated signalling pathways in the regulation of cranial suture morphogenesis and calvarial bone development. *Development*. **125**:1241–1251.
19. Franceschi, R.T., Iyer, B.S., and Cui, Y. 1994. Effects of ascorbic acid on collagen matrix formation and osteoblast differentiation in murine MC3T3-E1 cells. *J. Bone Miner. Res*. **9**:843–854.
20. Garcia Abreu, J., Coffinier, C., Larrain, J., Oelgeschlager, M., and De Robertis, E.M. 2002. Chordin-like CR domains and the regulation of evolutionarily conserved extracellular signaling systems. *Gene*. **287**:39–47.
21. Murphy-Ullrich, J.E., and Poczatek, M. 2000. Activation of latent TGF-beta by thrombospondin-1: mechanisms and physiology. *Cytokine Growth Factor Rev*. **11**:59–69.
22. Hall, K.B., and Horstadius, S. 1988. *The neural crest.* Oxford University Press. Oxford, United Kingdom. 305 pp.